A NUMERICAL PROCEDURE FOR THE VIRTUAL COMPRESSION AFTER IMPACT ANALYSIS

Rosario Borrelli[1], Stefania Franchitti[1], Francesco Di Caprio[1], Fulvio Romano[1], Umberto Mercurio[1,2]

[1]CIRA – Italian Aerospace Research Centre, Via Maiorise snc, 81043, Capua, Italy
[2]Technological District on Engineering of Polymeric and Composite Materials and Structures - IMAST, Italy

*Author to whom correspondence should be addressed: r.borrelli@cira.it

Received 16 January 2015; accepted 11 June 2015

ABSTRACT

The aim of the proposed research activity is to investigate on the structural behaviour of composite plates in order to develop numerical models able to describe their damage resistance to impact loads and their damage tolerance through compression after impact (CAI) test.The present paper presents a two-step simulation approach for determining the residual strength after a low velocity impact on a composite laminate of aeronautical interest. The first step is aimed at determining the damage extent after the impact event and it is performed by using an explicit finite element code. Hence, the damage status induced by the impact is transferred to the finite element model for the virtual compression after impact test which is simulated in a second step by using an implicit finite element code. Numerical results, in terms of force vs. displacement impact curve, damage envelope and reaction vs. applied strain compression curve, were compared to the experimental ones for validation purpose.

Keywords: Compression after Impact, Composite Material, Low velocity impact, damage resistance, damage tolerance, residual strength.

1. INTRODUCTION

All structure and components are likely to sustain impacts during service. It is vital that the reduction in performance caused by a "normal" impact is not so large as to make the item unsafe. Fibre-reinforced polymer composites, especially CFRP, are very susceptible to accidental impact damage and to reductions in strength. For compression loaded structures, the reduction in strength due to impact damage can be important and it is typically accounted for in design through the use of conservative material design allowable. Furthermore the damage tolerance of a structure must be repeatedly demonstrated throughout the design process from the coupon level to full-scale structural testing. Competition between aeronautical constructors has stimulated the massive use of composites in primary structures (Airbus 350 or Boeing 787), increasing significantly the attention that research programs have given to the problems related to the impact response and post-impact residual strength.

In the past, a lot of effort has been spent on the prediction of the impact damage and residual strength of impacted composite structures. Abrate gives a good overview of impact studies on composite materials in his book [1] and his survey papers [2, 3]. Considerable experimental studies [4 - 9] have been devoted to the problem with the aim of improving impact tolerance. In [4] and [5], low velocity impact and compression after impact (CAI) tests of four different laminate composite panels were carried out. It was found that the delaminated area is a function of the impact energy and is relatively independent of the stacking sequences used in that study. Furthermore, the residual strength when considered in terms of failure load depends on the stacking sequence, but the failure strain does not. Composites laminates of various in-plane dimensions and thicknesses were examined in [6] with regards to impact and post-impact behavior. Results showed that in-plane dimensional effect was not as significant as thickness effect. A new test method for evaluating the residual compression strength of composite after impact was proposed in [7], while the effect of resin and fibre properties on composite impact and CAI performances has been studied in [8]. Impact response of the laminates was found strongly influenced by the fracture toughness of the resin. In contrast, the use of high strength and high stiffness fibres did not improve the resistance to impact. An investigation of the effect of the impact location (central, near edge and on the edge) was made in [9]. The low velocity impact and CAI characterization of woven composite laminates were carried out in [10 - 13], while the CAI performance of stitched and unstitched cross-ply laminates were investigated in [14]. Finally, the use of composites in the manufacture of cryogenic fuel tanks for future reusable launch space vehicles was the motivation for the study performed in [15]

on the CAI performance at low temperature of composite laminates subjected to low-velocity impact.

At each step of the certification process of composite structural components, a combination of testing and analysis techniques is typically performed [16] since only the testing can be prohibitively expensive due to the large number of specimens needed to verify every geometry, loading, environment and failure mode. Therefore developments of reliable analysis tools for the prediction of both the impact response and the residual strength are very important in order to assess and improve structures. Simulation approaches allow trend observations on the reduction of residual strength with increasing impact energy or changes in impactor shape and size. Residual strength prediction can also be used in design tools to optimize for instance the lay-up of the laminate with non-conventional angles. In literature the prediction of residual strength of composite structures is approached in different ways.

The difficulties in facing this kind of problem, from a numerical point of view, stay in the fact that the prediction of the impact response and the prediction of its evolution under the service loads belong to two different disciplines. Such disciplines are usually indicated with the terms "damage resistance" and "damage tolerance" and have historically travelled independently to each other: the impact event is a dynamic one and it is better simulated by using FE code based on explicit time integration scheme. On the other hands, service loads are usually applied in a quasi-static way making the use of implicit code more appropriate. For these reasons, many authors proposed to predict the residual strength of impacted composite laminates by replacing the real and complex impact damage with a simpler "artificial" equivalent damage like delamination [17 -19] or open hole [20, 21]. Thus, the damage tolerance of the structure is investigated by including these equivalent defects in a simulation approach for determining the residual strength. In [22], the damage induced by a low velocity impact on a composite sandwich structure, including permanent indentation and delamination, measured from the real specimen, were all incorporated into the nonlinear finite element model simulating the compression after impact test and predicting the residual strength of the panel. An analytical model to predict the damaged zone due to an impact event is proposed in [23] where it is suggested to use this predicted damaged zone as basic input data for predicting the CAI strength of circular composite plates.

Only in a few works, the complete process (two-step simulation) of both impact simulation and residual compression strength simulation is presented. In [24], two methodologies for the prediction of the low-velocity impact response, impact damage and residual compressive strength of composite structures, are presented. The two methodologies, one for preliminary design and the other one for detailed design, have been developed and implemented in two in-house software programs and validated against experimental data. A complete study on the effect of fibre orientations on the impact and post impact compression behavior of straight fibre and variable angle tow laminates is presented in [25]. Impact and CAI simulations were performed both with an explicit code in order to enhance the understanding of the interaction between material orientation, matrix cracks and delaminations. Advanced progressive damage models are used in the works [26 -28] to predict delamination and in-plane damage growth during impact and post-impact events. In these works, the post-impact residual behavior is investigated by using the same explicit code employed to study the impact response even if the applied loads are applied in a quasi-static mode.

In the present work, a two-step simulation approach for determining the residual strength after a low velocity impact is investigated by using two different codes, one for the prediction of the impact response (explicit code) and the other one for the simulation of the CAI test (implicit code). The second stage in the approach uses the impact damage distribution which is transferred to the implicit code by a macro written by using the ANSYS® Parametric Design Language (APDL). The two-step simulation approach was applied to simulate the standardized CAI test (ASTM D7136 [29] and ASTM D7137 [30]) on a composite laminate of aeronautical interest. The virtual testing procedure was developed within the context of the project PRADE, funded by the Italian Ministry of University and Research (MIUR), and it was validated against experimental data obtained within the context of the project SMAF (SMart AirFrame) funded under the National Programme for Aerospace Research (PRORA).

2. TEST CASE DESCRIPTION

The scope of this paper is to develop a numerical procedure aimed at simulating and supporting the experimental tests ASTM D7136 [29] and ASTM D7137 [30]. These tests allow measuring the residual strength of a laminate through two separate steps:

Drop-weight impact test, according to the standard regulation [29], aimed at inducing damage into the composite laminates;

Compression after impact test, according to the standard regulation [30], to determine the residual compression strength.

The experimental tests have been performed on carbon fibre reinforced composites specimens with dimensions 100 x 150 mm and 5.012 mm thick. A sketch of the specimen and of the impact test configuration is shown in Fig. 1. Four rubber-tipped clamps restrain the specimen over a rigid fixture base and an hemispherical impactor drops vertically with a certain impact energy. In the present

study, two different energy levels (30 J and 50 J) were investigated.

According to the material reference system shown in Fig. 1, the laminates have the following stacking sequence: [45/-45/45/-45/0/0/90/0/0/45/-45/0/90/0]s, for a total of 28 plies. The material properties of the unidirectional lamina are summarised in Table 1.

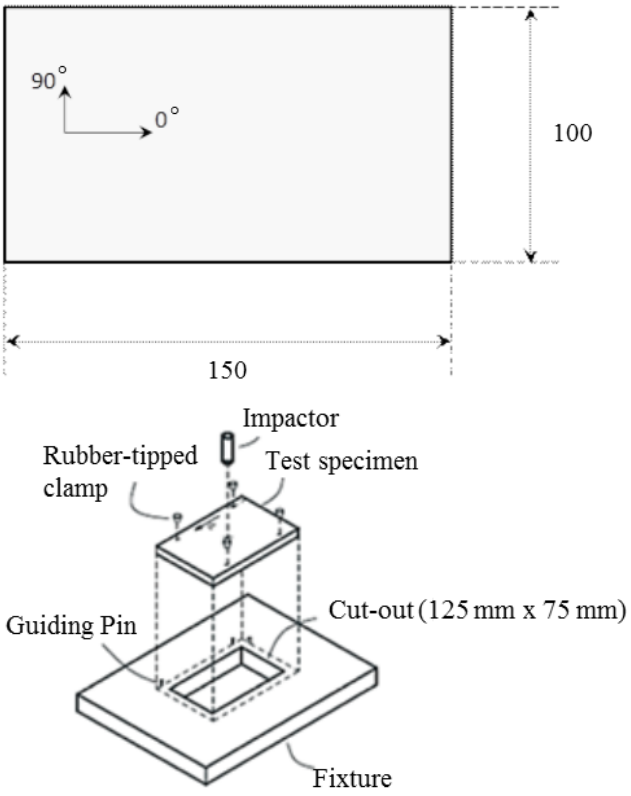

Fig. 1: Specimen dimensions (mm) and sketch of the impact test [29].

Table 1: Material Properties

Property	Symbol	Value	Units
Ply thickness	t_ply	0.179	mm
Density	ρ	1600	Kg/m^3
Longitudinal Young's modulus	E_1	149.5	GPa
Transverse Young's modulus	E_2	8.430	GPa
In-plane Shear modulus	G_{12}=G_{13}	4.2	GPa
Out-of-plane shear modulus	G_{23}	2.52	GPa
Poisson's ratio	ν_{12}, ν_{13}	0.33	
Longitudinal Tensile Strength	Xt	2143	MPa
Longitudinal Compressive Strength	Xc	968	MPa
Transverse Tensile Strength	Yt	75	MPa
Transverse Compressive Strength	Yc	250	MPa
Shear Strength	Sc	95	MPa

Both impact tests, at 30 J and 50 J, were performed by using the CEAST FRACTOVIS machine with an hemispherical impactor of mass equal to 8.64 kg and diameter equal to 20.0 mm. At each energy level, five specimens were tested and an high repeatability was found. Results in terms of force, displacement and absorbed energy time histories will be shown in the next sections compared to numerical results for validation purpose. Moreover, non destructive investigations were carried out after the impact tests in order to measure the damaged area due to the impact event.

The compression after impact tests were performed at room temperature and under displacement control by using the MTS 810 servo hydraulic testing machine. As prescribed by the standard regulation, an anti-buckling device, shown in Fig. 2, was used to avoid the onset of instability, thus, a pure compression failure was guaranteed. The compression load was applied along the largest dimension of the specimen which is the 0° laminate direction. Strain gage sensors were used to monitor the deformation and the reaction vs. applied strain curve, shown in the next sections, were compared to numerical results for validation purpose. In order to evaluate the compression strength of the pristine specimen, compression tests were also performed on non-impacted specimens. Such tests were named Compression Before Impact (CBI) tests. By comparing the failure strain of the impacted specimens with that one of the non-impacted specimen, it was found a Knock Down Factor (KDF) of 49% and 40% for the 50 J and 30 J test, respectively.

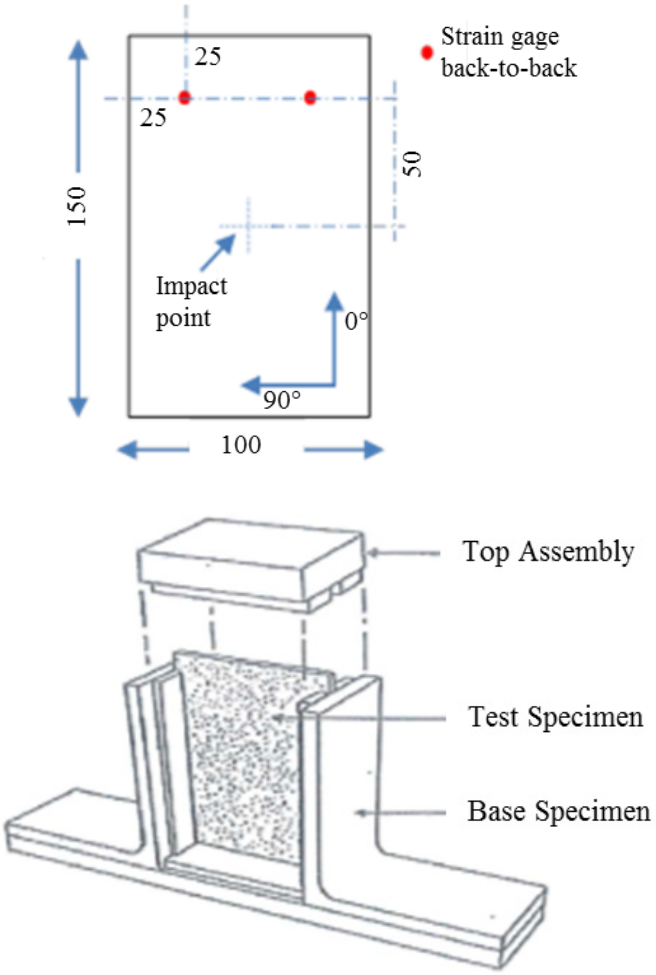

Fig. 2: Sketch of the CAI test according to the ASTM D7137 (dimension in mm) [30].

3. IMPACT ANALYSIS

The FEM model, developed in LS-DYNA for the simulation of the impact test, is shown in Fig. 3a and it was a results of an investigation presented in [31] aimed at developing a FEM model reproducing the impact response of a composite laminate.

As the plate length and width dimensions are large compared to the thickness, a 2D modelling approach was chosen. In particular layered fully integrated shell elements were used with an element length of 3.125 mm as a results of a sensitivity mesh analysis performed in [32].

The linear-elastic composite material model MAT54, available in the LS-DYNA library, was adopted to take into account for intralaminar damage (fibre and matrix failures) onset and propagation. The progressive failure analysis capability of MAT54 is based on the Chang-Chang failure criteria [33] which distinguishes between tensile FIBRE failure, compressive FIBRE failure, tensile matrix failure and compressive matrix failure. The elastic material behavior of the individual ply is calculated based on the input of the Young's modulus, shear modulus and Poisson's ratio. Damage occurs as soon as one of the following four criteria by Chang/Chang is met:

Tensile FIBRE failure:

$$e_{f,t}^2 = \left(\frac{\sigma_1}{X_T}\right)^2 + \beta\left(\frac{\tau_{12}}{S_C}\right)^2 - 1 \begin{cases} \geq 0 \; failure \\ < 0 \; elastic \end{cases} \quad (1)$$

Compressive FIBRE failure:

$$e_{f,c}^2 = \left(\frac{\sigma_1}{X_C}\right)^2 - 1 \begin{cases} \geq 0 \; failure \\ < 0 \; elastic \end{cases} \quad (2)$$

Tensile matrix failure:

$$\boldsymbol{e_{m,t}^2 = \left(\frac{\sigma_2}{Y_T}\right)^2 + \left(\frac{\tau_{12}}{S_C}\right)^2 - 1 \begin{cases} \geq 0 \; failure \\ < 0 \; elastic \end{cases}} \quad (3)$$

Compressive matrix failure:

$$\boldsymbol{e_{m,c}^2 = \left(\frac{\sigma_2}{2S_C}\right)^2 + \frac{\sigma_2}{Y_C}\left(\frac{Y_C^2}{4S_C^2} - 1\right) + \left(\frac{\tau_{12}}{S_C}\right)^2 - 1 \begin{cases} \geq 0 \; failure \\ < 0 \; elastic \end{cases}} \quad (4)$$

where XT and XC are the strength values for tension and compression in fibre direction, YT and YC in matrix direction. SC is the shear strength. The parameter β can be used to scale the shear stress interaction in the fibre tensile failure criterion. In this study a value of β=0.04 was used according to [32].

In addition to these stress-based criteria, failure strains can be defined as well. The stress level after meeting the Chang/Chang criteria is kept at a constant level until the failure strains are reached. Then the respective layer is assigned with zero stiffness properties. The constant levels are set by the user as a percentage of the strength values by using stress reduction factors (SLIM factors) for each failure mode. In this work, the factor for determining the constant stress level after tensile failure (both FIBRE and matrix failure) was set to 0.23 while the factor for determining the constant stress level after compressive failure (both FIBRE and matrix failure) was set to 0.30.

Inside one-shell element a number of sub-layers, representing the laminate lay-up, can be defined in thickness direction by using a certain number of through the thickness integration points. Usually each single ply is defined by one integration point and the check for intralaminar damage is carried out for all the through the thickness integration points. Once all the single integration points of the shell element have failed, the whole element is eroded, i.e. deleted from the calculation [34].

The separation of adjacent plies due to normal or shear loads, referred to as delamination, absorbs impact energy and decreases the laminate stiffness and therefore needs to be covered by the model as well. Because delaminations cannot be represented inside the continuum shell elements, in this work the laminate was divided into a certain number of sublaminates with tiebreack contacts in-between, which can fail during the simulation according to a specified failure law. To evaluate the influence of the number of shell elements layers in the stacked shell model, or in other words the number of delamination contact interfaces in-between, model with 2, 3, 7, 17 and 28 layers of shell elements across the thickness were generated with delamination contact definitions in-between. A model with just 1 layer of elements shell without delamination was also investigated.

The most realistic description of the phenomenon was provided by the model built according to the "difference in orientation of adjacent plies" criterion: in this proposed criterion adjacent plies with a difference in orientation lower than 90° were grouped into a unique layer of shell elements, on the other hands, adjacent plies with a difference in orientation equal to 90°, that is where delamination is most likely to occur, were separated by tiebreack contact definition (option 8).

For the laminates under investigation, the criterion led to a 17 layer FE model which was fine enough to accurately take into account the most significant interlaminar damage mechanisms inside the laminate. The tiebreack contact definitions allows to model interlaminar damage. After defined normal and shear failure stresses (NFLS and SFLS) are met, damage is a linear function of the distance of two points initially in contact. As soon as a defined critical crack opening (CCRIT) is reached, the contact is released

and converted in a regular surface-to-surface contact preventing penetrations. The energy release rates GIC and GIIC for normal and shear interface failure are approximated by:

$$G_{IC} = \frac{1}{2} NFLS * CCRIT \quad (5)$$

$$G_{IIC} = \frac{1}{2} NFLS * CCRIT \quad (6)$$

The 17 layers FE model was chosen in the present work for the complete process of both impact and residual compression strength simulation.

The fixture support and the hemispherical impactor were defined as rigid bodies since they are stiff steel parts whose stresses and strains distribution are not of interest. In order to capture the effect of the impactor drop, the impactor was modeled just before the impact position by specifying an initial impact velocity (vz=3.37 m/s for 50 J and vz=2.60 m/s for 30 J) consistent with the height of the free fall. A very fine mesh was adopted for the impactor in order to correctly compute the contact force between the impactor and the plate. An automatic surface-to-surface contact based on the standard penalty formulation was defined between the composite plate and the rigid impactor. The presence of the four rubber-tipped clamps was taken into account into the model by constraining the out-of-plane displacement of the nodes belonging to the upper layer of the specimen and positioned under the clamps as shown in Fig. 3b. In order to avoid lability and enforce the symmetry in the mechanical behavior, the x-displacement was constrained for the nodes at the centre of the AB and DC edges, while the y-displacement was constrained for the nodes at the centre of the BC and DA edges. The analyses were performed by using the Intel Xeon CPU E5450 quad-core processor and the total cpu time was about 2 hours for both 30J and 50J.

Results of the impact analysis, in terms of force vs. time, impactor displacement vs. time, absorbed energy vs. time and contact force vs. impactor displacement curves, are compared with experimental results (average values between the five tests) in Fig. 4 for the 50 J impact test.

The numerical and experimental comparison shows rather contained deviations. In particular the model was found able to accurately reproduce the peak of the force (Fmax≈16 kN), the contact duration (t≈5.0 ms), the critical load at which the first damage is induced (first drop in the force vs. time curve at about 9.8 kN) and the final energy (about 24 J) which is an indicator for the energy absorbed by the plate (dissipated for damage generation) during the impact. As matter of fact, the energy curves increase continuously to a maximum and fall to a certain level. This residual value is the measure of the absorbed energy, which is not transferred to the impactor as elastic springback. If the plate behaved completely elastic without failure and neglect the friction losses, the energy curve would return to zero again. The comparison between numerical results and experimental ones (average values between the five tests) for the impact test at 30 J is shown in Fig. 5. A good correlation of the main parameters was found again.

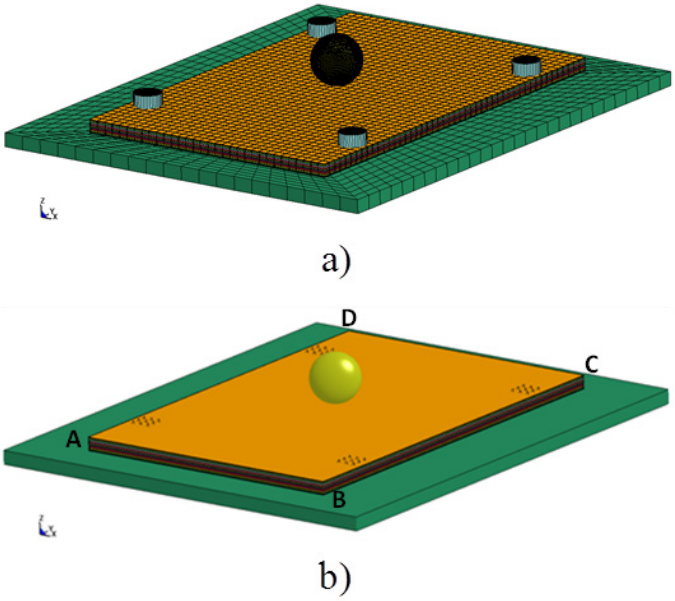

Fig. 3: (a) FEM model and (b) boundary conditions.

In Fig. 6, the numerical damage envelope is shown for the 30 J and for the 50 J impact test. The numerical damage envelope was computed by a macro written by using the ANSYS® Parametric Design Language (APDL) which checks for both interlaminar and intralaminar damage:

For the intralaminar damage, the macro checks the damage variable of each failure mode (FIBRE tensile, FIBRE compression, matrix tensile and matrix compression) for all the integration points through the thickness of each finite element. If failure is found the element is plotted in red, intact element are plotted in cyan blue.

For the interlaminar damage, the macro checks for released tiebreack nodes in each interface. Due to numerical oscillations, spurious tiebreack nodes are released making the interlaminar damage distribution not too much feasible. Hence, in this work, only when three adjacent nodes are released from the tiebreack contact definition, the respective element is considered delaminated and plotted in red. The measured numerical damaged areas for both energy levels correlates quite well with those ones measured from NDI evaluation. In particular, the damaged areas for the impact test at 30 J and 50 J are 1133 mm2 and 2266 mm2, respectively. They are estimated with an error of +7.9% for the 30 J and -0.7% for the 50 J with respect to the experimental data.

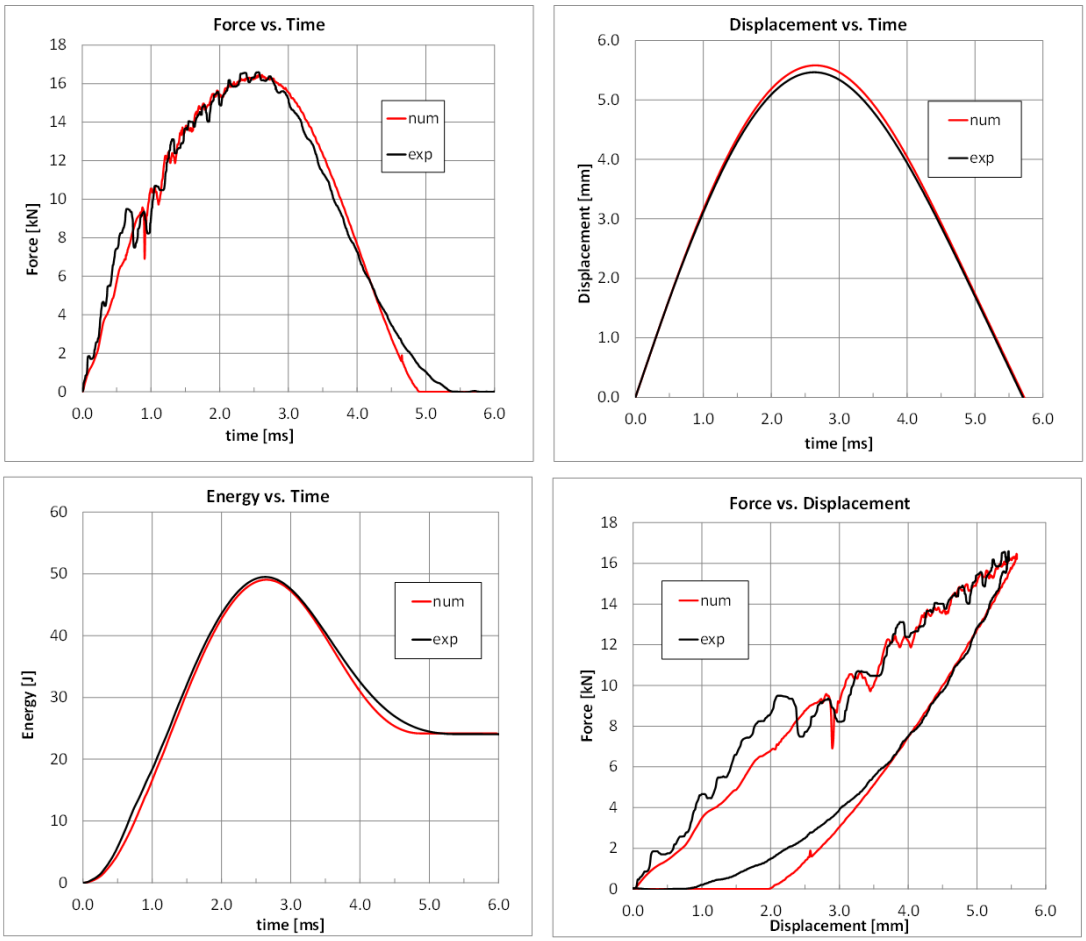

Fig. 4: Numerical vs. Experimental results – Impact at 50 J.

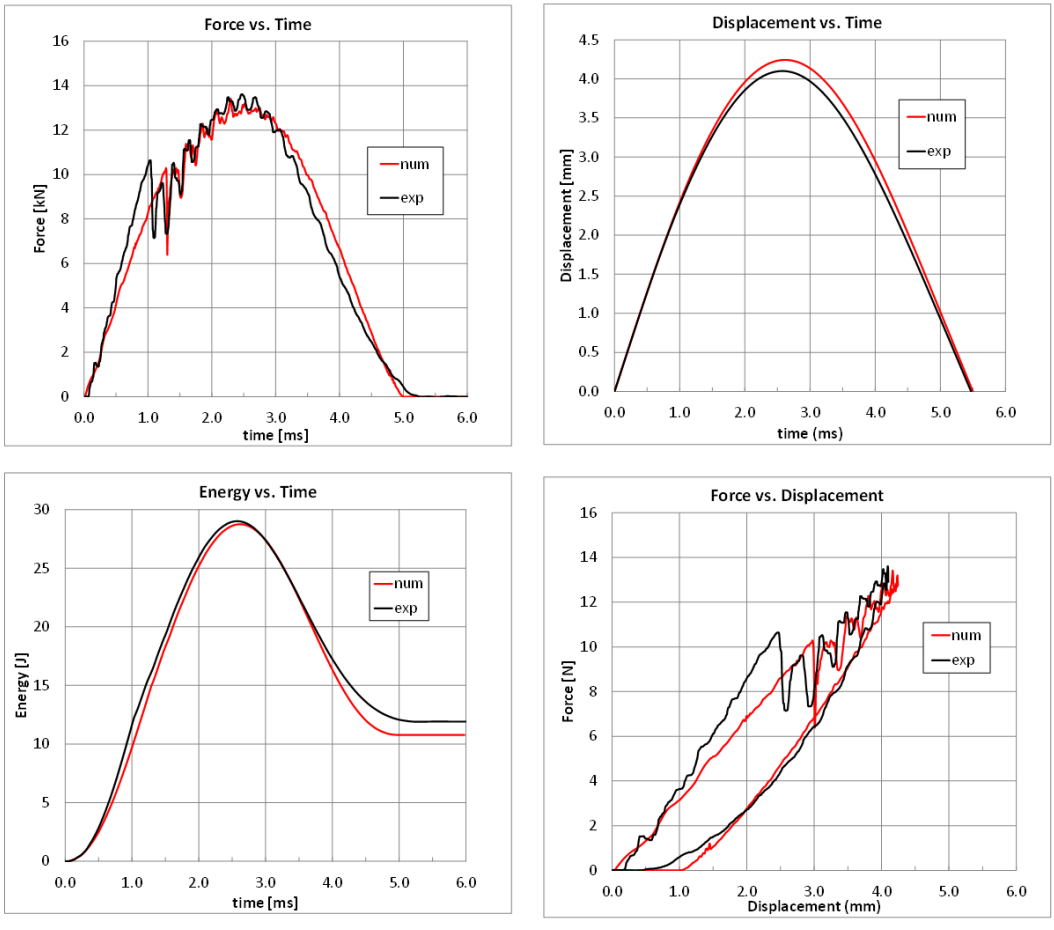

Fig. 5: Numerical vs. Experimental results – Impact at 30 J.

The macro allows also to map the intralaminar damage distribution in each sublaminate. As an example, the intralaminar damage distribution for the upper sublaminate (the 17th one), which is loaded in compression during the impact event, is plotted in Fig. 7. The figure on the left side is the intralaminar total damage envelope relative to the 17th sublaminate while the figures on the right side are the damage distribution for each intralaminar failure mode. As expected, the compressive fibre failure is the most predominant failure mode for that sublaminate and happens along the 45 degree diagonal where the maximum deformation has been obtained.

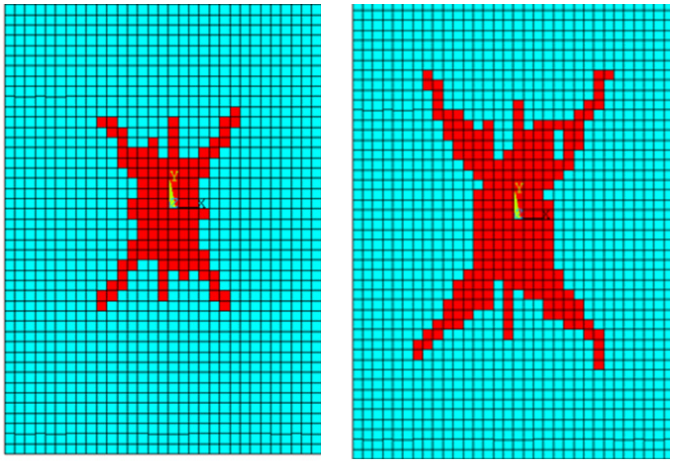

a) b)

Fig. 6: Numerical damage envelope at 30 J (a) and 50 J (b).

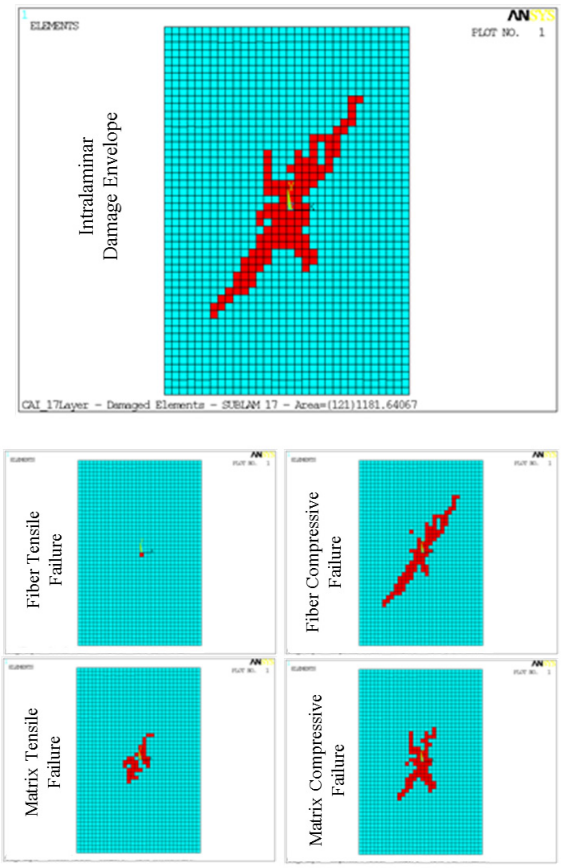

Fig. 7: Intralaminar damage distribution for the 17th sublaminate.

4. DAMAGE TRANSFER PROCEDURE

The damage distribution induced by the impact analysis should be transferred to the ANSYS® model for the subsequent compression after impact analysis. To this aim, another subroutine written in APDL was developed. Such subroutine receives in input the impact damage information which are mapped in a monolayer layered shell ANSYS® model (one layer of shell through the thickness) for the compression analysis. In the compression model, each ply of the laminate is defined by one through the thickness integration point. To take into account the damage induced by the previous impact analysis, each single integration point, and thus each ply, is associated to different sets of material properties. In particular, each single integration point through the thickness of a generic finite element is associated to one of the following materials having different identified (mid):

mid 10= pristine material properties as reported in Table 1;
mid 11= degraded material properties due to FIBRE breackage;
mid 12= degraded material properties due to matrix failure;
mid 13= degraded material properties due to both FIBRE breackage and matrix failure.

The material properties of mid 11, mid 12 and mid 13 are degraded with respect to the pristine material properties according to the degradation rules reported in Table 2 [35 -36]. As an example, if the impact analysis has found a matrix failure in the ith ply of a certain element, then the ith ply of the corresponding element of the ANSYS® model is associated to mid 12 with transversal Young modulus (E_{22}) and the shear modulus (G_{23}) degraded with respect to the pristine value by using the degradation factor k which can be chosen by the user.

Table 2: Degradation rules applied during damage transfer.

Failure mode	Degradation rules
Fibre failure	$\overline{E}_{11} = (1-k)\cdot E_1$
	$\overline{G_{12}} = G_{23}$
	$\overline{G_{13}} = G_{23}$
Matrix failure	$\overline{E}_{22} = (1-k)\cdot E_2$
	$\overline{G_{23}} = (1-k)\cdot G_{23}$

Hence, the damage status generated by the impact event in a certain area of the specimen is taken into account by using degraded material properties in that zone. It should be highlighted that while the intralaminar damage is incorporated in the ANSYS® model, the delamination information is not. Nevertheless, since during the compressive test the collapse of the plate is triggered by FIBRE failure [26] such limit of the numerical procedure proposed in this work does not represent a big issue. However, within the

context of ongoing research programs, an attempt to improve the procedure taking into account both intralaminar and interlaminar damages is making.

5. COMPRESSION AFTER IMPACT ANALYSIS

The 4-node structural layered shell element "shell181", available in the ANSYS® library [37], was used for the compression analysis. The FEM is shown in Fig. 8 where red elements are associated to a degraded material model. In order to simulate the real boundary conditions experienced during the experimental test, the following constraints were applied:

uy=uz=rotx=0 for all the nodes belonging to the edge AB. Moreover, for the central node of this edge, also ux was set to zero;

uz=roty=0 for all the nodes belonging to the edges BC and AD;

uz=rotx=0 and uy=-1.5 mm for all the nodes belonging to the edge CD. Moreover, for the central node of this edge, also ux was set to zero.

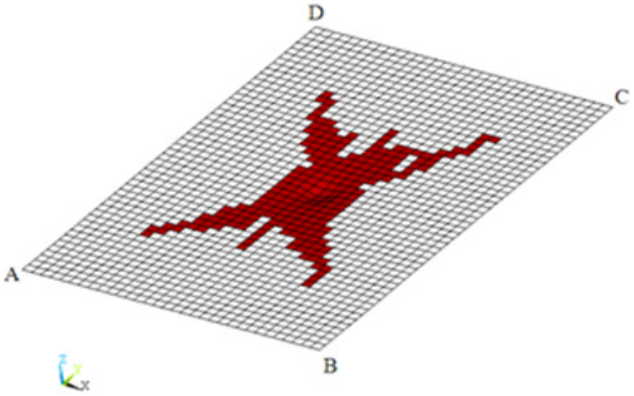

Fig. 8: ANSYS® FE model for compression after impact analysis.

Once transferred the impact damage status to the ANSYS® FE model, the CAI analysis was performed by using the progressive failure analysis ANSYS® capability. The progressive damage model, known as ply-discount damage model, is described by the flowchart of Fig. 9. At each load step, a non linear analysis is performed until a converged solution is obtained. Then, using this equilibrium state, the stress distribution in each lamina is computed and stored. The stresses are introduced into specified failure criteria, which are then checked to determine whether any failures have occurred or not. If the adopted failure criterion indicates that lamina failure has occurred, the lamina properties are degraded according to a particular degradation model. Since the initial nonlinear solution no longer corresponds to an equilibrium state due to the fact that material properties have been degraded, equilibrium of the structures needs to be re-established utilizing the modified lamina properties for the failed lamina while keeping the current load level. This iterative process of obtaining nonlinear equilibrium solutions each time a local material model is changed is continued until no additional lamina failures are found. The load step is then incremented until catastrophic failure of the structure is detected (converged solution is no more obtained).

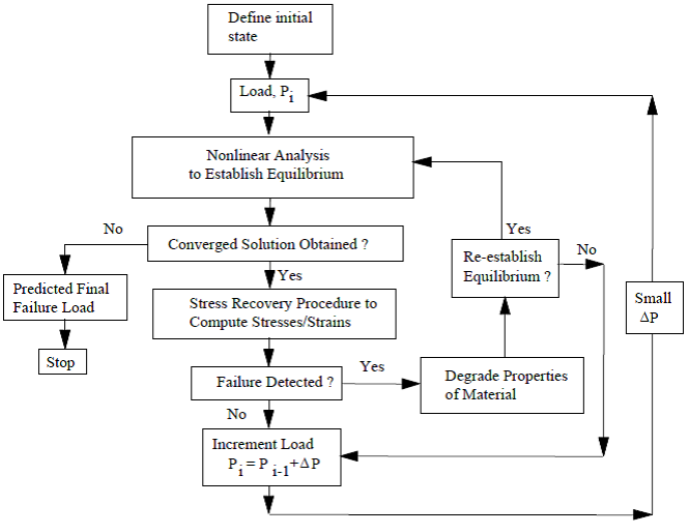

Fig. 9: Flowchart of a typical progressive failure analysis.

Hence, the efficiency of a progressive failure model is based on the appropriate selection of two ingredients: the type of the failure criterion utilized to evaluate the failure initiation and the material degradation model implemented to decrease the load carrying capability of the damaged structure. In this work, the Hashin failure criteria [38] which distinguish between several failure modes (tensile FIBRE, compressive FIBRE, tensile matrix and compressive matrix) were used to determine failure initiation. Furthermore, instant-stiffness-reduction evolution laws were utilized to define the way a material degrades.

According to these laws, one or more of the elastic material properties of a lamina are set to be equal to zero once failure is detected. Nevertheless, in practice, a small value for the material properties is retained in order to avoid difficulties in the nonlinear analysis solution [39].

The ANSYS® degradation model assumes that the stiffness reduction associated with damage due to tensile loads is different from the stiffness reduction associated with damage due to the compressive loads. Moreover, it is assumed also that there could be a difference from the way a material degrades in the fibre direction to the one in the matrix direction. This means that the following four stiffness reduction coefficients needs to be defined:

C1=Tensile fibre stiffness reduction coefficient;
C2=Compressive fibre stiffness reduction coefficient;
C3=Tensile matrix stiffness reduction coefficient;
C4=Compressive matrix stiffness reduction coefficient.

When damage occurs, the material properties associated with the detected mode of failure are degraded according to the following rule:

Table 3: Degradation rule during progressive failure analysis.

Failure Mode		Degradation rules
Fibre failure (tension)	$\sigma_{xx} > 0$	$\overline{E}_1 = (1-C_1)\cdot E_1$
Fibre failure (compression)	$\sigma_{xx} < 0$	$\overline{E}_1 = (1-C_2)\cdot E_1$
Matrix failure (tension)	$\sigma_{yy} > 0$	$\overline{E}_2 = (1-C_3)\cdot E_2$
Matrix failure (compression)	$\sigma_{yy} < 0$	$\overline{E}_2 = (1-C_4)\cdot E_2$

In the present work, the capability to define different damage evolution laws for each failure mode was not investigated, and, according to [39-42], it was assumed that C1=C2=C3=C4=C. Moreover, in order to be consistent with the damage transfer procedure, such coefficient was set equal to the degradation factor k used to transfer the impact damage to the ANSYS® model.

A limited sensitivity analysis with respect to the coefficient k ranging from k=0.950 to k=0.999 was performed for the 50 J impact test case. In Fig. 10, the results of this sensitivity study in terms of computed failure load are reported.

It was found that the model is not sensible to the degradation factor k in the range 0.980-0.999 and results obtained in this range are in good agreement with the mean experimental load. For the subsequent analyses presented in this work, according to literature [39], it was chosen to use the degradation factor value belonging to the range where k was found insensitive and which, at the same time, provides less convergence problems. Such value was k=0.980.

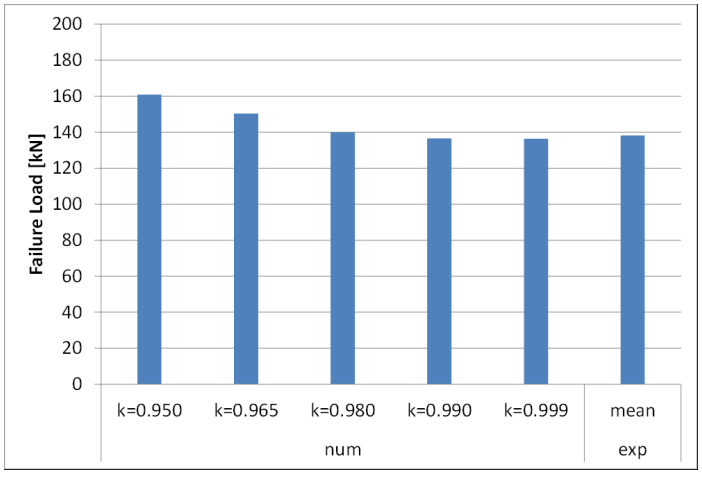

Fig. 10: Influence of degradation factor on the failure load for the CAI test at 50 J.

In Fig. 11, a comparison between the experimental and numerical results, in terms of load vs. applied strain curve, is shown for both the Compression After Impact (CAI) at 50 J and the Compression Before Impact (CBI) tests. As far as the experimental curves are concerned, the average curves obtained from five compression tests are reported. On the other hands, both numerical curves plotted in Fig. 11 with continuous lines, simulating the CAI and CBI tests, were obtained by using the degradation factor k=0.980.

The main failure load (245 kN) and the stiffness of the undamaged specimens was well predicted by the FE model. Also, the mean failure load (138 kN) and the stiffness of the 50 J impacted specimen was well reproduced by the virtual CAI procedure developed in this work.

Finally, with the aim of verifying its robustness, the numerical virtual CAI procedure was applied to the 30 J impact test case by setting again the degradation factor equal to 0.980. In Fig. 12, the numerical load vs. applied strain curve is compared to the experimental results (mean curve). In this case, the failure load is underestimated of 5.9% with respect to the mean experimental value (157 kN).

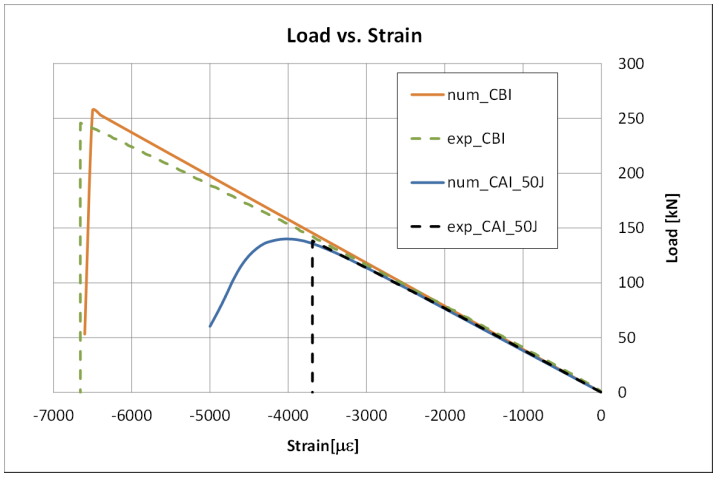

Fig. 11: Load vs. applied strain for CAI (50 J) and CBI test.

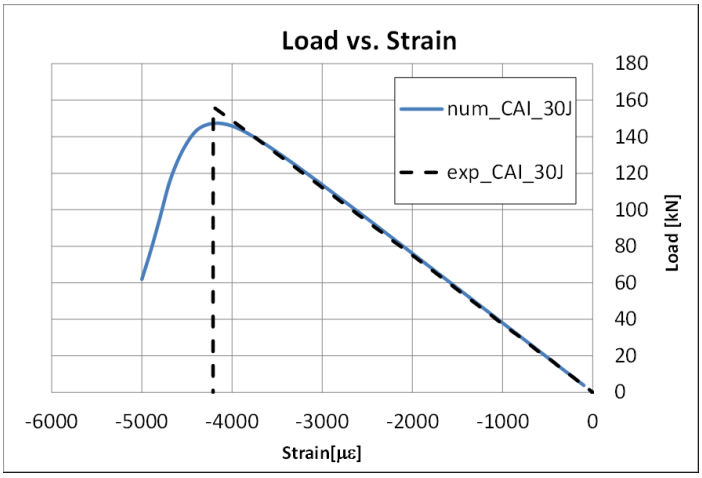

Fig. 12: Load vs. applied strain for CAI (30 J).

6. CONCLUSIONS

An LS-DYNA – ANSYS® coupled procedure was proposed to simulate the impact and the Compression After Impact test performed according to the ASTM standard regulations on composite laminated plates. The procedure was validated against an experimental database. The con-

sidered numerical techniques allow to estimate damages and residual compressive strength in good agreement with experimental results. In the future the robustness of this procedure with respect to different layups and thicknesses will be considered using a more large experimental database. The development and validation of such virtual test procedure could lead to significant benefits in the industrial applications. First of all, during the certification process, the virtual test procedure allows to reduce the number of experimental tests which are quite expensive. Moreover, the procedure allows also to reduce conservatism in the design process of composite structure and thus to reduce the structure weight and the operative costs.

ACKNOWLEDGEMENTS

This work was partially performed in the frame of the project PRADE (PON02_00029_3205863) granted to IMAST S.c.a.r.l. and funded by the Italian Ministry of Education, Universities and Research (MIUR).

Authors would like to kindly thank Prof. Antonio Langella from University of Naples Federico II and Ph.D. Cinzia Toscano from the Advanced Technologies and Materials CIRA laboratory for their precious support to the experimental activity.

References:

1. Abrate, S., "Impact on composite stuctures", Cambridge University Press, 1998.
2. Abrate, S., "Impact of composite laminates", Appl Mech Rev 1991; 44: 155-190.
3. Abrate, S., "Impact of composite laminated composites: recent advances", Appl Mech Rev 1994; 47: 517-544.
4. Reis, L. and De Freitas, M., "Damage growth analysis of low velocity impacted composite panels", Compos Struct 1997; 38: 509-515.
5. De Freitas, M. and Reis, L., "Failure mechanisms on composite specimens subjected to compression after impact", Compos Struct 1998; 42: 365-373.
6. Liu, D., Raju, B.B. and Dang, X., "Size effects on impact response of composite laminates", Int J of Imp Engin 1988, 21(10): 837-854.
7. Habib, F.A., "A new method for evaluating the residual compression strength of composites after impact", Compos Struct 2001; 53: 309-316.
8. Cartiè, D.D.R. and Irving, P.E., "Effect of resin and fibre properties on impact and compression after impact performance of CFRP", Compos Part A 2002; 33: 483-493.
9. Malhotra, A. and Guild, F.J., "Impact Damage to Composite Laminates: Effect of impact location", Appl Compos Mater 2014. DOI: 10.1007/s10443-013-9382-z
10. Naik, N.K., Joglekar, M.N., Arya, H., et al., "Impact and compression after impact characteristics of plain weave fabric composites: effect of plate thickness", Adv Compos Mater 2004, 12(4): 261-280.
11. Reyes, G. and Sharma, U., "Modeling and damage repair of woven thermoplastic composites subjected to low velocity impact", Compos Struct 2010; 92: 523-531.
12. Aktas, M., Balcioglu, H.E., Aktas, A., et al., "Impact and post impact behavior of layer fabric composites", Compos Struct 2012; 94: 2809-2818.
13. Dale, M., Acha, B.A. and Carlsson, L.A., "Low velocity impact and compression after impact characterization of woven carbon/vinylester at dry and water saturated conditions", Compos Struct 2012; 94: 1582-1589.
14. 1Aymerich, F. and Priolo, P., "Characterization of fracture modes in stitched and unstiched cross-ply laminates subjected to low-velocity impact and compression after impact loading", Int J of Imp Engin 2008, 35: 591-608.
15. Sanchez-Saez, S., Barbero, E. and Navarro, C., "Compressive residual strength at low temperatures of composite laminates subjected to low velocity impacts", Compos Struct 2008; 85: 226-232.
16. EASA AMC 20-29. Composite Aircraft Structure 2010.
17. Aoki, Y. and Kondo, H., "Effect of delamination propagation on mechanical behavior in compression after impact", In: 16th International Conference on Composite Materials, Kyoto, Japan, 2007
18. 1Riccio, A. and Tessitore, N., "Influence of loading conditions on the impact damage resistance of composite panels", Comp and Struct 2005; 83: 2306-2317.
19. Sala, G., "Post-impact behavior of aerospace composites for high-temperature applications: experiments and simulations", Compos Part B 1997; 28B: 651-665.
20. Hawyes, V.J., Curtis, P.T. and Soutis, C., "Effect of impact damage on the compressive response of composite laminates", Compos Part A 2001; 32: 1263-1270.
21. Soutis, C. and Curtis, P.T., "Prediction of the post-impact compressive strength of CFRP laminated composites", Compos Sci Technol 1966; 56: 677-684.
22. Zonghong, X., Vizzini, J. and Qingru, T., "On Residual Compressive Strength Prediction of Composite Sandwich Panels after low-velocity impact damage", Acta Mech. Solida Sinica 2006; 19 (1): 9-16.
23. Lee, J. and Soutis, C., "Prediction of impact-induced fibre damage in circular composite plates", Appl Compos Mater 2005; 12: 109-131.
24. Karger, L., Baaran, J., Gunnion, A., et al., "Evaluation of impact assessment methodologies. Part I: Applied methods", Compos: Part B 2009; 40: 65-70.
25. Dang, T.D. and Hallett, S.R.., "A numerical study on impact and compression after impact behavior of variable angle tow laminates", Compos Struct 2013; 96: 194-206.
26. Gonzales, E.V., Maimì, P., Camanho, P.P., et al., "Simulation of drop-weight impact and compression after impact tests on composite laminates". Compos.Struct 2012; 94: 3364-3378.
27. Bouvet, C., Rivallant, S. and Hongkarnjanakul, N., "Failure analysis of composite laminate subjected to impact and compression after impact". In: Workshop Understanding Failure Mechanisms of Composites for Sustaining and Enhancing Military Systems Structures, Riga, Latvia, 7-9 October 2013.
28. Van den Brink, W.M., Van de Vrie, G. and Nawijn, M., "Post-Impact Residual Strength Analysis of Composite Aerospace Structures using Progressive Damage Methods", In: Workshop Understanding Failure Mechanisms of Composites for Sustaining and Enhancing Military Systems Structures, Riga, Latvia, 7-9 October 2013.
29. ASTM D7136: "American Standard Test Method for measuring the damage resistance of a fibre-reinforced polymer matrix composite to a drop-weight impact".
30. ASTM D7137: "Standard Test Method for Compressive Residual Strength Properties of Damaged Polymer Matrix Composite Plates".

31. Borrelli, R., Franchitti, S., Di Caprio, F., et al., "A CAE Based Procedure to Predict the Low Velocity Impact Response of a Composite CAI Specimen", In: International CAE Conference 2013, Verona, Italy, 21-22 October.
32. Heimbs, S., Heller, S., Middendorf, P., et al., "Low velocity impact on CFRP plates with compressive preload: Test and modelling", Int J Imp Engin 2009, 36: 1182-1193
33. Chang, F.K. and Chang, K.Y., "A progressive damage model for laminated composites containing stress concentrations", J Compos Mater 1987; 21: 834-855.
34. LS-DYNA® Version 971 R6.1.0, keyword User's Manual, Volume II material models.
35. Perugini, P., Riccio, A. and Scaramuzzino, F., "Three-dimensional progressive damage analysis of composite joints", In: Proceedings of the Eighth International Conference on Civil and Structural Engineering Computing, 2001.
36. Murray, Y. and Schwer, L., "Implementation and verification of fibre-composite damage models, Failure Criteria and Analysis in Dynamic Response", ASME AMD 1990, 107, 21-30.
37. ANSYS® 14.5, Help Manual
38. Hashin, Z., "Failure criteria for unidirectional fibre composites", J Appl Mech 1980; 47: 329-334.
39. Riccio, A., "Effects of geometrical and material features on damage onset and propagation in single-lap bolted composite joints under tensile load: Part II – numerical studies", J Comp Mater 2005, 39(23): 2091-2112.
40. Riccio, A. and Pietropaoli, E., "Modeling Damage Propagation in Composite Plates with Embedded Delamination under Compressive Load". J Comp Materal 20008, 42(13): 1309-1335.
41. Pietropaoli, E. and Riccio, A., "A global/local finite element approach for predicting interlaminar and intralaminar damage evolution in composite stiffened panels under compressive load", Appl Compos Mater 2010, DOI: 10.1007/s10443-010-9135-1.
42. Sleight, D.W., "Progressive Failure Analysis Methodology for Laminated Composite Structures", NASA Techincal Paper 1999, NASA/TP-1999-209107.